Optical second-harmonic diffraction study of anisotropic surface diffusion: CO on Ni(110)

Xu-Dong Xiao, X. D. Zhu,* W. Daum,† and Y. R. Shen
Department of Physics, University of California, Materials Sciences Division, Lawrence Berkeley Laboratory, Berkeley, California 94720

(Received 3 February 1992; revised manuscript received 12 May 1992)

We describe in detail a technique using optical second-harmonic (SH) diffraction from a one-dimensional laser-induced monolayer grating to probe surface diffusion of adsorbates and its anisotropy on a solid surface. The case of CO on Ni(110) is used as a demonstration. The two orthogonal and independent diffusion tensor components along $[1\bar{1}0]$ and [001] are measured, exhibiting a strong anisotropy in both the activation energy $E_{\rm diff}$ and the preexponential factor D_0 in the diffusion coefficients. A compensation effect between $E_{\rm diff}$ and D_0 is observed. In comparison with CO/Ni(111) and CO/Ni(100), our result suggests that the Ni(110) surface seen by CO is much smoother than Ni(111) and Ni(100). Both advantages and limitations of the present technique are mentioned and possible complications in the data analysis are discussed.

I. INTRODUCTION

The study of heterogeneous surface diffusion is a fundamental step towards understanding the mechanism of many surface processes, ranging from associative desorption of adsorbates, epitaxial crystal growth, to catalysis.[1-3] It can also provide useful information about the effective surface potential and diffusion pathways experienced by adsorbates. On crystalline surfaces, the structural anisotropy is expected to effect anisotropy in surface diffusion. Anisotropic surface diffusion can cause preferential development of surface reactions in certain forms and is therefore important in the practical consideration of controlling surface reactions. Surprisingly, despite its importance, research effort on anisotropic surface diffusion so far has been rather limited. This is presumably due to limitation in the existing experimental techniques.

In the study of tracer surface diffusion (referring to motion of single atom or molecule on a surface), field-ion microscopy is commonly used. It allows very detailed measurements of diffusion kinetics of metal atoms on refractory metal substrates.[1-3] More recently, scanning tunneling microscopy has made the study of tracer surface diffusion on semiconductors possible.[4] Both techniques yield clear maps of the random motion of the adsorbates and hence the diffusion anisotropy. Theoretical understanding of tracer surface diffusion has also been fairly advanced. The application of molecular-dynamic simulations[5-10] with pairwise potentials between the adatom and substrate atoms, for example, has provided a good description of the diffusion process. The trajectory tracing procedure makes the diffusion paths very transparent. Mechanisms such as successive jumps, return jumps,[9] substrate deformation, and exchange of adatoms with substrate atoms (concerted exchange)[6] have been explored. Analytical theories based on both static and dynamic coupling of adatoms and substrate atoms have also been developed.[11,12]

The situation with chemical surface diffusion (referring to the motion of a large number of adsorbed atoms or molecules on a surface) is however very different. Because the adsorbate-adsorbate interaction can now be significant, the process is far more complicated. Yet, it is more important than tracer diffusion considering the relevance to practical applications. Unfortunately the complexity of the process has greatly impeded the progress in this field, especially on anisotropic surface diffusion. While theoretically, the difficulties arise from the necessity of taking into account both adsorbate-substrate and adsorbate-adsorbate interactions in the calculations, experimentally, the progress has been impeded to some extent by measuring techniques.

Several experimental probes have been developed to study anisotropic chemical surface diffusion. Work-function changes and scanning Auger electron microscopy have been used to measure anisotropic diffusion on metals,[1,13] but the initial coverage profile is hard to prepare and the measurement could be perturbed by the electric field or electrons present. The field emission method measuring fluctuation autocorrelation in a region restricted by a rectangular slit has been very successful.[14] However, the degree of anisotropy that can be measured is limited by the length/width ratio of the rectangular slit. Since the method relies on the separation of two correlation functions, only surfaces with C_{2v} symmetry have been studied. Furthermore, diffusion coefficients along arbitrary directions other than the principal axes of the surface cannot be directly measured. More recently, the scheme of hole burning by laser-induced thermal desorption (LITD) has also been employed to study surface diffusion.[15] It is possible to extend the method to anisotropic surface diffusion measurements by changing the desorption laser intensity profile from circular to rectangular. Again, the range of the anisotropy in the diffusion coefficient that can be measured by this technique is limited by the length/width ratio of the desorption profile. In addition, the LITD method requires an accurate determination of the coverage profile after desorption in order to determine the diffusion coefficient

from the measurement with reasonable accuracy. Because of the existing coverage gradient between the desorbed and undesorbed regions, it is also difficult to measure the coverage dependence of the diffusion coefficient. The other problem intrinsic to this method is that the high intensity laser pulses applied sequentially to probe, via laser desorption, surface diffusion by hole refilling could induce laser damage of the surface, thereby affecting the surface properties.[16]

Very recently, we have developed a technique employing optical diffraction from a monolayer grating to measure surface diffusion.[17,18] In this method we first burn a grating in the monolayer of adsorbates on a surface by laser desorption using two interfering laser beams. The monolayer grating can be probed by optical diffraction. As the adsorbates diffuse on the surface to smear out the grating, the diffraction signal decreases accordingly. From the decay of the diffraction, the diffusion coefficient can be deduced. In our experiments, we have used the first-order second-harmonic (SH) diffraction from the monolayer grating to monitor surface diffusion. It is well known that second-order nonlinear optical processes are highly surface specific. Thus, using SH diffraction to probe a monolayer grating has the advantage of effectively eliminating the background noise due to bulk scattering. The disadvantage is that the SH diffraction signal is rather weak, limiting the accuracy of the diffusion measurements.

The monolayer grating diffraction method has a number of very attractive features. First, it involves a simple one-dimensional diffusion process for which the data analysis is relatively straightforward. Second, by properly orienting the grating, the diffusion coefficient along any direction on the surface can be directly measured. This makes the anisotropic diffusion measurement easy and not limited. Third, as an optical method, the technique can be applied to a wide variety of adsorbates on any substrate. Fourth, with a tunable probe beam selectively probing particular species of adsorbates, surface diffusion of individual components of a mixed adsorbate layer can be monitored. This allows the study of influence of surface diffusion on surface reactions such as catalysis. Finally, the technique can be used to study other forms of surface diffusion like diffusion of electronic or vibrational excitations.

In this paper we present an anisotropic surface diffusion study using the monolayer grating diffraction method with SH diffraction as the probe. The system chosen to demonstrate the technique is CO/Ni(110). The main result has been reported earlier in a letter.[18] Here we include the details of our investigation. The Ni(110) surface has a row structure with atoms closely packed in the $[1\bar{1}0]$ direction (see Fig. 1). The CO molecules can adsorb with almost equal probabilities on both top- and short-bridge sites up to a coverage of $\theta=0.85$.[19] For $\theta>0.85$, the CO molecules are pushed to the top site to form zig-zag chains along the $[1\bar{1}0]$ rows with adjacent CO molecules displaced in the [001] and $[00\bar{1}]$ directions, respectively. At a full coverage, the tilt angle of CO molecular axis with respect to the surface normal is $\sim 20°$ and the adsorbate structure appears as 2×1.[20] Obviously, surface diffusion of CO on Ni(110) at all coverages must be anisotropic. At an average CO coverage of $\theta_0 \sim 0.5$ we can expect diffusion along $[1\bar{1}0]$ as jumping from top or short-bridge sites to short-bridge or top sites; and along [001] as jumping from top sites to top sites and from short-bridge sites to short-bridge sites. Thus one would anticipate the existence of two independent diffusion barriers, one along $[1\bar{1}0]$ and the other along [001]. They were indeed identified in our experiment. The diffusion energies and the preexponential factors for the two orthogonal directions were deduced. Both of them show strong anisotropy, namely, the diffusion energy is significantly larger along [001] than along $[1\bar{1}0]$, accompanied by a larger preexponential factor also along [001]. This correlation between the diffusion energy and the preexponential factor reminds us of the compensation effect that often happens in chemical or other reactions described by the Arrhenius behavior. Our results are however approximate since the coverage dependence of the diffusion coefficients has not been taken into account in the analysis.

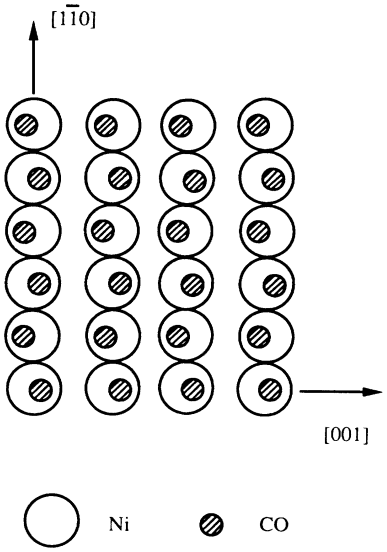

FIG. 1. Structure of the Ni(110) surface with a full monolayer of CO adsorbates. The CO monolayer has a symmetry of 2×1. The sizes of Ni atoms and CO molecules are not shown in proportion.

The organization of the paper is as follows: Section II describes the experimental details on sample preparation, creation of the CO monolayer grating by laser desorption, and measurement of the first-order SH diffraction from the grating. Section III gives the theoretical background of SH diffraction from the monolayer grating and how the decay of the diffraction relates to the one-dimensional diffusion of CO adsorbates. The experimental results of CO diffusion on Ni(110) are presented in Sec. IV, and discussed in Sec. V with the consideration whether surface defects, coverage dependence of the SH response, and coverage dependence of diffusion kinetics could affect the results from the data analysis. Finally, physical understanding of CO diffusion on Ni(110) will also be discussed in light of the present experimental findings.

II. EXPERIMENTAL TECHNIQUE AND ARRANGEMENT

A. Sample preparation

The experiment was performed in an ultrahigh-vacuum (UHV) chamber with a base pressure of 1.0×10^{-10} torr. The single-crystal Ni(110) sample was cut and mechanically polished to within 0.3° from the (110) plane with the miscut along the [001] direction, and mounted vertically on a rotatable sample holder capable of more than 90° of rotation about [110]. Before any measurement, the surface of the sample was first Ar^+ sputtered (at 1.0×10^{-4} torr with a 500-V beam voltage for approximately 30 min) at room temperature until no impurity contamination could be detected by the Auger electron spectrometer within its detection limit (<0.3% for carbon and <0.5% for sulfur). The sample was then annealed at 800 °C for a few seconds followed by a slow cooling down to the measurement temperature. Right before each dosing of CO the sample was flash heated to 300 °C to remove residual adsorbed molecules from the ambient, mostly hydrogen and CO. The adsorption of CO on the Ni(110) surface was carried out at approximately 100 K by introducing CO into the chamber through a leak valve. A sharp 1×1 low-energy electron diffraction (LEED) pattern was observed for a clean Ni(110) surface and a 2×1 pattern for a full CO monolayer on Ni(110). In order to avoid possible alternation of the surface and the adsorbate monolayer by the electron beam in the LEED measurement, separately prepared monolayers were used for diffusion experiment. A Chromel-Alumel thermal couple welded to the sample was used to monitor the sample temperature. The diffusion experiment was conducted in a temperature range of 100 to 170 K. The temperature could be controlled to within 2 K. The average CO coverage for all the diffusion experiments at different temperatures and in different directions was $\theta_0\sim0.5$, with $\theta=1$ defined as full CO coverage with one CO molecule per Ni atom on the surface.

B. Experimental considerations in making an adsorbate grating

The key step in preparing for our diffusion measurement was to create a CO monolayer grating that could yield a strong enough SH diffraction signal. This was achieved by LITD with a prescribed spatial intensity modulation formed by interfering two laser beams. The adsorbate grating profile can be predicted from the laser intensity modulation if the amount of CO desorbed versus desorbing laser energy is known in LITD. We used reflected second-harmonic generation (SHG) to find such a relation. First, the reflected SHG was measured as a function of CO exposure (pressure multiplied by time) to the surface. Then the CO coverage of the surface versus exposure was determined from thermal desorption spectroscopy.[21] Thus the relation between reflected SHG and CO coverage on Ni(110) was found. We were particularly interested in the adsorbate-induced SHG signal, or $|\Delta\chi^{(2)}_{\rm eff}(\theta)|^2$, as a function of coverage θ. As described in Ref. 22 this could be obtained by an interference technique. A p-in(fundamental)/p-out(SH) polarization geometry was chosen since this SHG signal was the strongest among all the different polarization combinations, knowing that $\chi^{(2)}_{zzz}(\theta)$ is the dominating component in the nonlinear susceptibility tensor. Finally, SHG was used to monitor LITD.

The setup for the LITD experiment is shown in Fig. 2, where the desorbing laser beam at 1.06 μm was aligned collinearly with the probing laser (for SHG) at 0.532 μm. The probing beam radius was one-tenth of that of the desorbing beam and probed the central uniform part of the desorbed area. The measured result of $|\Delta\chi^{(2)}_{\rm eff}(\theta)|^2$ is shown in Fig. 3 and the CO desorption yield from Ni(110) as a function of desorption energy is depicted in Fig. 4(a). The LITD result can be fitted with a laser heating model in which the adsorbed laser energy from the pulse is converted directly into heat to induce a temperature change.[23] The temperature rise is given by

$$\Delta T(t)=\frac{\Delta E}{\Delta A}(1-R)\cos\theta_{\rm inc}\frac{1}{\sqrt{\pi\tau_p}}\times\int_{-\infty}^{t}\frac{dt'}{\sqrt{\pi}\rho C_p K}\frac{\exp(-t^2/\tau_p^2)}{\sqrt{t-t'}}, \quad (1)$$

where $\Delta E/\Delta A$ is the laser intensity impinged on the surface, $R=0.728$ is the reflectance of Ni at the incident angle $\theta_{\rm inc}\sim45°$, $\tau_p=10$ ns is the Gaussian laser pulse width, and $\rho=8.902$ g/cm^3, $C_p=6.23$ cal/mol K, and $K=91$ W/m K are the density, heat capacity, and heat conductance of Ni, respectively.[24] Being a first-order desorption process, the desorption rate of CO from Ni(110) is assumed to be given by[25]

$$\frac{d\theta}{dt}=-\nu\theta e^{-E_{\rm des}/k_B T(t)}, \quad (2)$$

where ν is the desorption preexponential factor, $E_{\rm des}$ the desorption energy, and k_B the Boltzmann constant. Equation (2) then leads to the thermal desorption yield

$$\Delta\theta=\theta_s\left\{1-\exp\left[-\int_{-\infty}^{\infty}\nu e^{-E_{\rm des}/k_B T(t')}dt'\right]\right\}. \quad (3)$$

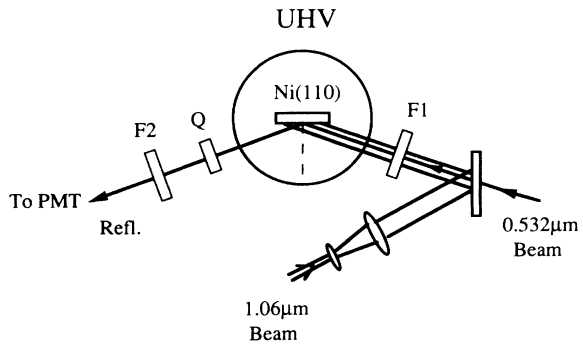

FIG. 2. Optical setup for experiment using optical second-harmonic generation to probe laser-induced thermal desorption. $F1$ and $F2$ are color filters and Q is a quartz plate employed to cancel the SHG signal from the bare Ni(110) surface by interference.

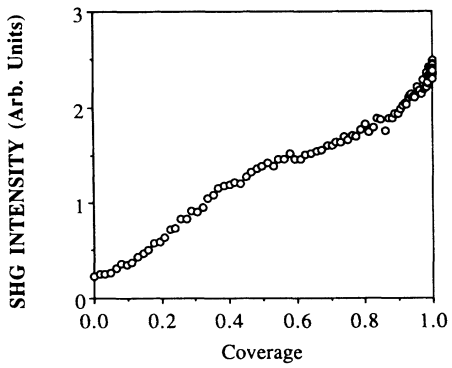

FIG. 3. $|\Delta\chi^{(2)}_{\text{eff}}(\theta)|^2$ vs coverage θ measured by SHG with the plane of incidence parallel to $[1\bar{1}0]$ and the p-in/p-out polarization combination.

The solid line in Fig. 4(a) is a fit of the data using Eqs. (1) and (3) with $\nu=1\times10^{14}$ and $E_{\text{des}}=28$ kcal/mol. The values of ν and E_{des} agree well with those obtained by other methods.[25] The discrepancy in the fit is presumably due to the fact that the coverage dependence of the desorption energy and the preexponential factor were neglected in the calculation.

To make a monolayer adsorbate grating, we interfered two laser beams at the Ni(110) surface to produce a spatially modulated intensity

$$I(x)=I_0\left[1+r\cos\left[\frac{2\pi x}{s}\right]\right], \tag{4}$$

where I_0 is the average intensity, s the grating spacing, r the contrast of the interference pattern, and x the position along the surface. In our experiment, I_0 was chosen such that $\Delta\theta(I_0)\sim0.5$. By adjusting the weak beam intensity to $0.08I_0$ to make $r=0.524$, the grating appeared to have a tripodal periodic pattern as sketched in Fig. 4(c). Such a pattern has a large first-order Fourier component that will produce a large first-order diffracted SH signal.

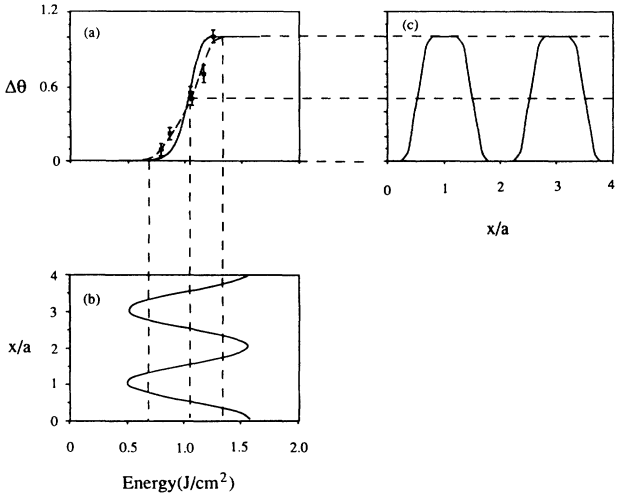

FIG. 4. (a) Desorption mass yield vs desorbing laser energy as measured by laser-induced thermal desorption. The solid line is a theoretical calculation from Eq. (3) with $\nu=1\times10^{14}$ and $E_{\text{des}}=28$ kcal/mol. The dashed line along the data points is a guide for the eye. (b) Laser energy distribution at the surface from two interfering laser beams. (c) The resulting coverage grating created by the laser energy distribution in (b).

We noticed from Fig. 4(a) that for CO/Ni(110), the energy range from no desorption to complete desorption is very narrow. Experimentally, this means that the formation of a good grating requires very accurate control of the laser energy.

C. Experimental setup for diffusion measurement

The optical arrangement for diffusion experiment is shown in Fig. 5. A single-mode Q-switched Nd:YAG (where YAG denotes yttrium aluminum garnet) laser with a pulse width of 10 ns at 1.06 μm was used for both the LITD and the SH diffraction measurements. To create a CO monolayer grating on Ni(110), the 1.06-μm beam was split into two and then recombined at incident angles of $\phi=\pm1.50°$ with an overlapping area of ~2 mm in diameter on the Ni(110) surface fully covered by CO. The choice of the ratio of the two beams and the average laser intensity were discussed earlier. The CO grating thus produced resembled the pattern described in Fig. 4(c), and the grating period was $s=\lambda/2\sin\phi\sim20$ μm.

To probe the diffusion, a frequency-doubled laser beam at 0.532 μm from the Nd:YAG laser was used. Its intensity was $\sim\frac{1}{10}$ of the desorbing beam. The beam was incident at 70° with respect to the surface normal and the first-order SH diffraction from the CO grating was detected as a function of time in order to probe the decay of the CO grating via CO diffusion. The probe beam was not strong enough to desorb CO from Ni, as could be checked by monitoring SHG in the specularly reflected direction. Alternatively, this was made sure by creating a CO adsorbate grating in the [001] direction at ~100 K and monitoring the change in the first-order SH diffraction. No change was found for several hours, indicating that diffusion, desorption, and adsorption of CO

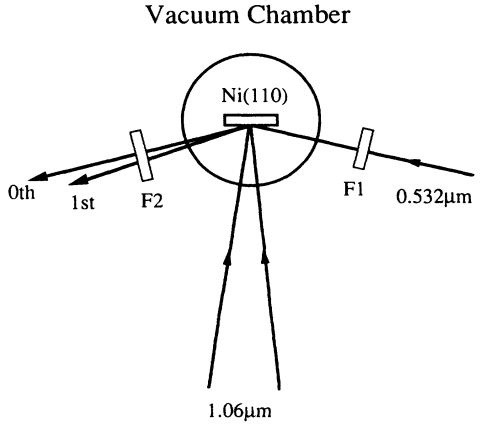

FIG. 5. Experimental setup for surface diffusion experiment. A single laser shot at 1.06 μm is always used to generate an adsorbate grating. The decay of the grating is monitored by the first-order SH diffraction using the 0.532-μm probe beam.

are all negligible in that circumstance. The diffusion coefficient could be deduced from the decay of the diffracted SH signal.

In an earlier work, we reported a similar diffusion study for CO on the Ni(111) surface.[17] In comparison, the CO-induced SHG from Ni(110) is 4–5 times smaller than that from Ni(111).[22,26,27] The desorption energy range is also very narrow for CO on Ni(110) as compared to CO on Ni(111).[23] In the present case, the desorption laser energy has to be controlled to within 2–3 % of 1.24 J/cm^2 in order to create a good grating that can yield a reasonable SH diffraction level ($\sim$80 counts/5 min, with $S/N\sim 10$ in our measurement). These reasons make the surface diffusion experiment of CO/Ni(110) rather difficult. Moreover, for gratings along different crystalline orientations, the SH diffraction signal may differ by about 10% because the p-in/p-out SH response with the plane of incidence parallel to different crystalline directions involve different components of the second-order nonlinear susceptibility tensor $\overleftrightarrow{\chi}^{(2)}(\theta)$. For instance, $\chi^{(2)}_{\rm eff}$ is a linear combination of $\chi^{(2)}_{zzz}$, $\chi^{(2)}_{xzx}$, and $\chi^{(2)}_{zxx}$ if the plane of incidence is parallel to $[1\bar{1}0]$ and a linear combination of $\chi^{(2)}_{zzz}$, $\chi^{(2)}_{yzy}$, and $\chi^{(2)}_{zyy}$ if the plane of incidence is parallel to [001]. This anisotropy in signal strength, however, will not affect the diffusion coefficient measurement since it is the decay rate that determines the diffusion coefficient as we will see in Sec. III.

The diffusion anisotropy was measured in the following way. For measurement of CO diffusion along a selected direction on Ni(110), the sample was rotated to have that direction in the plane of incidence of the desorbing laser beams. The CO monolayer grating on the surface could then be created by the method described above. The diffusion measurement along such a chosen direction was subsequently carried out at a few temperatures in order to find the temperature dependence of the diffusion coefficient $D(T)$. Measurements were performed for CO diffusion not only along the principal axes of Ni(110) but also along other directions of interest.

III. RELATIONS BETWEEN DIFFUSION COEFFICIENT AND THE SH DIFFRACTION SIGNAL

Surface diffusion is generally characterized by a rank-2 diffusion coefficient tensor $\overleftrightarrow{\mathrm{D}}$ which is related to the particle flux $\mathbf{J}$ and the surface coverage θ by

$$\mathbf{J}=-\overleftrightarrow{\mathrm{D}}\cdot\nabla\theta \ . \tag{5}$$

The tensor can be diagonalized along symmetry axes in the surface. For the case of Ni(110) the axes for diagonalization are $[1\bar{1}0]$ and [001], so that we have

$$\overleftrightarrow{\mathrm{D}}=\begin{bmatrix} D_{[1\bar{1}0]} & 0 \\ 0 & D_{[001]} \end{bmatrix} . \tag{6}$$

Thus for surface diffusion along a direction at an angle ϕ away from $[1\bar{1}0]$, the diffusion coefficient is given by

$$D(\phi)=D_{[1\bar{1}0]}\cos^2\phi+D_{[001]}\sin^2\phi \ . \tag{7}$$

As discussed in the preceding section, we are interested in observing surface diffusion from the time-dependent smearing of a monolayer grating of adsorbates. In this case, surface diffusion is governed by the one-dimensional diffusion equation

$$\frac{\partial\theta}{\partial t}=\frac{\partial}{\partial x}\left[D\frac{\partial\theta}{\partial x}\right] , \tag{8}$$

and the solution can be expressed in terms of a Fourier series expansion:

$$\theta(x,t)=\theta_0+\sum_{n=1}^{\infty}\theta_n(t)\cos(2n\pi x/s) \ . \tag{9}$$

If D is assumed to be independent of the coverage θ, then we find,

$$\theta(x,t)=\theta_0+\sum_{n=1}^{\infty}\theta_n^0\cos(2n\pi x/s)\exp(-4n^2\pi^2Dt/s^2) \ , \tag{10}$$

where θ_n^0 are constants. More generally, D depends on θ and the solution becomes more complicated. This will be discussed later in Sec. V.

The nonlinear susceptibility $\chi^{(2)}_{\rm eff}(\theta)$ responsible for SHG from a CO covered Ni(110) surface can be separated into two parts, one from the bare metal substrate, and the other from the adsorbate-induced contribution which depends on coverage:

$$\chi^{(2)}_{\rm eff}(\theta)=\chi^{(2)}_{\rm eff}(0)+\Delta\chi^{(2)}_{\rm eff}(\theta) \ . \tag{11}$$

If $\theta(x)$ is periodic in x, then $\chi^{(2)}_{\rm eff}(\theta)$ is also periodic in x, and can be written as

$$\chi^{(2)}_{\rm eff}[\theta(x)]=\chi^{(2)}_{\rm eff}(0)+\sum_{n=0}^{\infty}A_n(t)\cos(2n\pi x/s) \tag{12}$$

with

$$A_n=\lim_{L\to\infty}\frac{2}{L}\int_{-L/2}^{L/2}\chi^{(2)}_{\rm eff}[\theta(x)]\exp\left[i\frac{2n\pi x}{s}\right]dx \ . \tag{13}$$

SHG from such a susceptibility grating appears both in specular reflection and in diffraction. The specularly reflected SH signal is proportional to $|\chi^{(2)}_{\rm eff}(0)+A_0|^2$ and the nth-order diffracted SH signal is proportional to $|A_n|^2$.

Consider the simple case that $\Delta\chi^{(2)}_{\rm eff}(\theta)$ is linearly proportional to the coverage θ. Then $A_n\propto\theta_n$ and the nth-order SH diffraction is given by

$$S_n(t)\propto|\theta_n|^2=S_{0n}\exp(-8\pi^2n^2Dt/s^2) \ . \tag{14}$$

From the time constant of the exponential decay of the diffracted SH signal, the diffusion coefficient D can be deduced. Note that the decay time constant is independent of the grating pattern except the grating spacing s. If $\Delta\chi^{(2)}_{\rm eff}(\theta)$ is not linearly proportional to θ, the situation again becomes more complicated as $S_n(t)$ is no longer proportional to $|\theta_n(t)|^2$. The decay of $S_n(t)$ would appear as multiexponential. This will be discussed in the Sec. V.

IV. EXPERIMENTAL RESULTS

The measured data of the first-order SH diffraction signal versus time from CO monolayer gratings on Ni(110) along three different directions, $[1\bar{1}0](\phi=0°)$, $[001](\phi=90°)$, and $\phi=45°$ are presented in Figs. 6(a), 6(b), and 6(c), respectively. Assuming that Eq. (14) is valid, we fit the data at each temperature by a single exponential, as shown by the solid curves in Fig. 6. From the fit and using Eq. (14) with $n=1$, we can deduce the decay time constant and hence the diffusion coefficient $D(T)$ (with $s=20$ μm). The fluctuation of the data points was mainly due to the poor signal-to-noise ratio. The uncertainty in determining the diffusion coefficient D is around $\pm 40\%$.

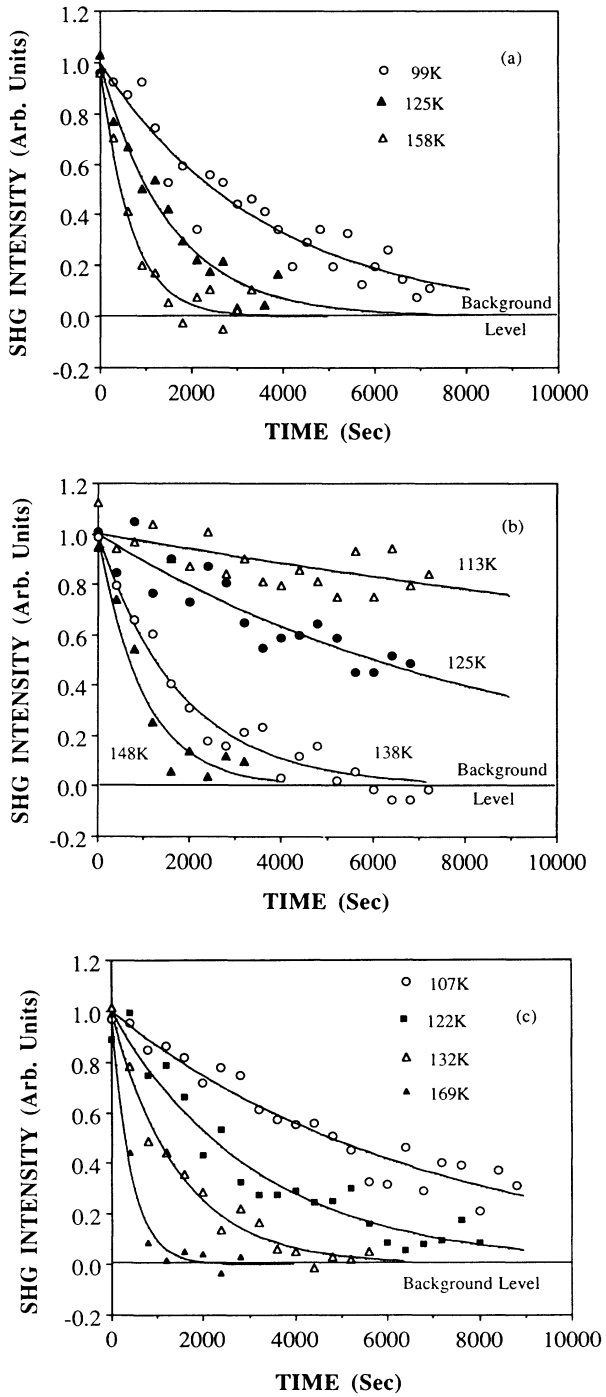

FIG. 6. Normalized first-order SH diffraction signal vs time at different temperatures for CO diffusion along (a) $[1\bar{1}0]$, (b) [001], and (c) the direction bisecting $[1\bar{1}0]$ and [001] on the Ni(110) surface. The solid lines are the exponential fits with Eq. (14).

The deduced diffusion coefficient D vs $1/T$ is plotted in Fig. 7 for CO diffusion along the three specific directions on Ni(110). The results for diffusion along the orthogonal directions, $[1\bar{1}0]$ and [001], are well described by the simple Arrhenius form

$$D=D_0\exp(-E_{\rm diff}/k_BT)\ . \tag{15}$$

This indicates that CO diffusion on Ni(110) has two distinct potential barriers, one along $[1\bar{1}0]$ and the other along [001]. The fit of Eq. (15) to the data points in Fig. 7 yields, along $[1\bar{1}0]$

$$E_{\rm diff}([1\bar{1}0])=1.1\pm0.2\ \text{kcal/mol}\ (0.048\ \text{eV})\ ,$$

$$D_0([1\bar{1}0])=(3.8\pm2.0)\times10^{-9}\ \text{cm}^2/\text{sec}\ ;$$

along [001],

$$E_{\rm diff}([001])=3.1\pm0.4\ \text{kcal/mol}\ (0.134\ \text{eV})$$

$$D_0([001])=(4.8\pm4.4)\times10^{-6}\ \text{cm}^2/\text{sec}\ .$$

That surface diffusion of CO on Ni(110) is anisotropic is obvious from the above results. For diffusion along the direction $\phi=45°$, we expect from Eq. (7)

$$D(\phi=45°)=\tfrac{1}{2}(D_{[1\bar{1}0]}+D_{[001]})\ . \tag{16}$$

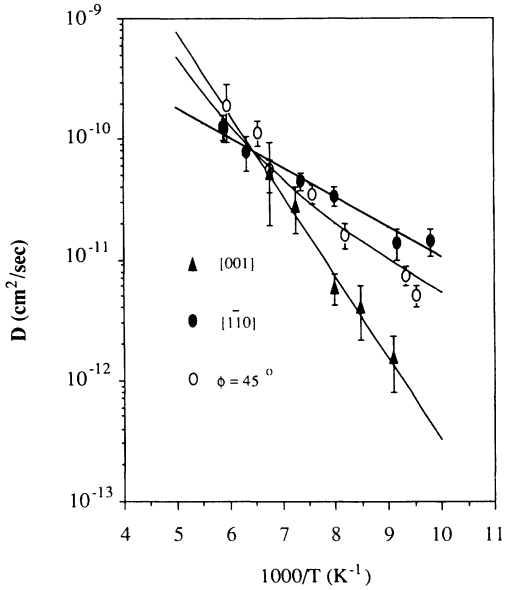

FIG. 7. Diffusion coefficient D vs reciprocal temperature $1/T$ in an Arrhenius plot for CO diffusion on Ni(110) along $[1\bar{1}0]$, [001], and the direction bisecting the two ($\phi=45°$). The solid lines are least-square fits by Eqs. (15) and (16) with $E_{\rm diff}[1\bar{1}0]=1.1$ kcal/mol, $D_0[1\bar{1}0]=3.8\times10^{-9}$ cm^2/sec, and $E_{\rm diff}[001]=3.1$ kcal/mol; $D_0[001]=4.8\times10^{-6}$ cm^2/sec.

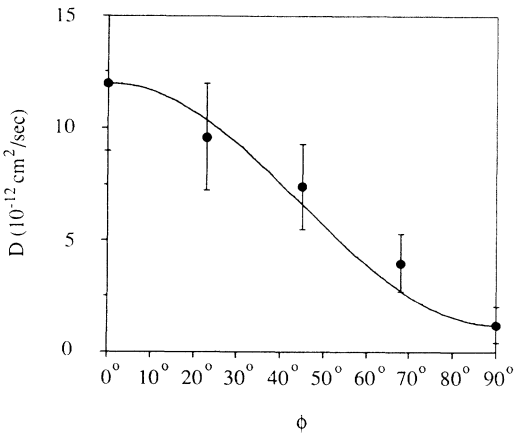

FIG. 8. Diffusion coefficient D for CO/Ni(110) as a function of azimuthal angle ϕ away from $[1\bar{1}0]$ at $T\sim 110$ K. The solid line is calculated from Eq. (7) using the diffusion parameters deduced from Fig. 7.

Plotted in Fig. 7, Eq. (16) fits the experimental data very well. Note that two combined exponential functions of $1/T$ are needed to describe $D(\phi=45°)$. This further supports the picture of two orthogonal independent diffusion barriers for CO on Ni(110).

Figure 8 depicts the measured D as a function of the diffusion direction specified by ϕ at fixed temperature $T\sim 110$ K. The solid curve calculated from Eq. (7) is also in good agreement with the data. The diffusion anisotropy at $T=110$ K is obviously very significant.

V. DISCUSSION

In deducing the diffusion coefficient D from our experiment, we have made a number of simplifying assumptions (see Sec. III). In this section, we shall first consider the effects of those assumptions and other possible experimental complications before we discuss the implication of the experimental results.

A. Heating effect from the probing beam

One may wonder if the laser beam used to probe the monolayer grating would heat up the sample surface and significantly affect the surface diffusion of the adsorbates. In our measurements, the fluence of the probe laser pulse was ~ 0.1 J/cm^2. Using Eq. (1) in Sec. II, we estimate a maximum temperature rise of 65 K for the Ni surface at $t\sim 10$ ns due to laser heating. This temperature rise decays away to $\Delta T<10$ K at $t\sim 40$ ns. From Eq. (15), we find $D(T+\Delta T)/D(T)=10-500$ for a temperature range of $T\sim 100-170$ K with $\Delta T=65$ K if $E_{\rm diff}=3.1$ kcal/mol. The excess mean-square displacement resulting from $D(T+\Delta T)$ during the heating period of $\delta t\sim 40$ ns is given by

$$\Delta\langle x^2\rangle=\int_0^{\delta t}2\{D(T+\Delta T)-D(T)\}dt\sim 2D(T+\Delta T)\delta t\ .$$

This is negligible compared to the mean-square displacement $2D(T)\Delta t$ of CO molecules during the period $\Delta t=0.1$ s between two successive laser pulses. For smaller $E_{\rm diff}$, the effect is even smaller. Thus we can conclude that the probe laser heating effect is insignificant in our surface diffusion measurements.

B. Coverage dependence of nonlinear susceptibility

In the data analysis, we assumed $\Delta\chi^{(2)}_{\rm eff}(\theta)$ is linear in θ. This is not true, in general, and is a poor approximation for CO on Ni(110) as seen in Fig. 2. As mentioned briefly in Sec. III, the nonlinear relation between $\Delta\chi^{(2)}_{\rm eff}(\theta)$ and θ may cause the first-order SH diffraction to decay multiexponentially or nonexponentially. This can be seen by expanding $\Delta\chi^{(2)}_{\rm eff}(\theta)$ into power series of $(\theta-\theta_0)$, where θ_0 is the average surface coverage of the monolayer grating.

$$\Delta\chi^{(2)}_{\rm eff}(\theta)=\Delta\chi^{(2)}_{\rm eff}(\theta_0)+\left[\frac{d\Delta\chi^{(2)}_{\rm eff}}{d\theta}\right]_{\theta_0}(\theta-\theta_0)+\frac{1}{2}\left[\frac{d^2\Delta\chi^{(2)}_{\rm eff}}{d\theta^2}\right]_{\theta_0}(\theta-\theta_0)^2+\frac{1}{6}\left[\frac{d^3\Delta\chi^{(2)}_{\rm eff}}{d\theta^3}\right]_{\theta_0}(\theta-\theta_0)^3+\cdots\ . \tag{17}$$

From Eq. (13), the first-order SH diffraction amplitude takes the form

$$A_1(t)=\left[\frac{d\Delta\chi^{(2)}_{\rm eff}}{d\theta}\right]_{\theta_0}\theta_1^0\exp(-t/2\tau)+\frac{1}{2}\left[\frac{d^2\Delta\chi^{(2)}_{\rm eff}}{d\theta^2}\right]_{\theta_0}\sum_{m=1}\theta_m^0\theta_{m+1}^0\exp\{-[m^2+(m+1)^2]t/2\tau\}+\frac{1}{8}\left[\frac{d^3\Delta\chi^{(2)}_{\rm eff}}{d\theta^3}\right]_{\theta_0}\left[\sum_{(m,n)=1}\theta_m^0\theta_n^0\theta_{m+n+1}^0\exp\{-[m^2+n^2+(m+n+1)^2]t/2\tau\}+\sum_{(m,n)=1}\theta_m\theta_n\theta_{m+n-1}\exp\{-[m^2+n^2+(m+n-1)^2]t/2\tau\}\right]+\cdots\ , \tag{18}$$

where $\tau=s^2/8\pi^2D$ and D is assumed constant. Since generally, $\theta^0_{m+1}<\theta^0_m<1/2$ for $m>1$, we expect that the higher-order terms can be appreciably smaller than the first term in Eq. (18). The two leading correction terms are $\frac{1}{2}(d^2\Delta\chi^{(2)}_{\rm eff}/d\theta^2)_{\theta_0}\theta_1^0\theta_2^0\exp(-5t/2\tau)$ and $\frac{1}{8}(d^3\Delta\chi^{(2)}_{\rm eff}/d\theta^3)_{\theta_0}(\theta_1^0)^3\exp(-3t/2\tau)$. For $t>\tau/2$, they are further reduced by factors larger than e^{-1} and $e^{-1/2}$, respectively. Thus we can conclude that if $\Delta\chi^{(2)}_{\rm eff}(\theta)$ can be approximated by a power-series expansion of Eq. (17) and if the data analysis puts more emphasis on the diffraction data at later times, then a single-exponential decay of the diffraction with $\Delta\chi^{(2)}_{\rm eff}(\theta)$

$=\Delta\chi^{(2)}_{\rm eff}(\theta_0)+(d\Delta\chi^{(2)}_{\rm eff}/d\theta)_{\theta_0}(\theta-\theta_0)$ is a fair approximation. In principle, one can make the grating groove sufficiently shallow to render $\Delta\chi^{(2)}_{\rm eff}(\theta)\propto(\theta-\theta_0)$ so that the decay would certainly be a single exponential. Unfortunately, limited by the diffraction signal strength which is proportional to $|\Delta\chi^{(2)}_{\rm eff}(\theta)|^2$, this may not always be possible.

For the case of CO on Ni(110), the experimental data of $\Delta\chi^{(2)}_{\rm eff}(\theta)$ can be approximated by (see Fig. 2)

$$\Delta\chi^{(2)}_{\rm eff}(\theta)\propto 0.707+0.707(\theta-\theta_0)-0.354(\theta-\theta_0)^2 +0.354(\theta-\theta_0)^3+\cdots \quad (19)$$

with $\theta_0=0.5$. If we assume an initial CO monolayer grating of the rectangular periodic form

$$\theta(x)=0.5+\sum_{n=1}^{\infty}\frac{2}{n\pi}\sin\left[\frac{n\pi}{2}\right]\cos(2n\pi x/s)\ , \quad (20)$$

then we can show from Eq. (18) that by keeping only the first term in Eq. (18), the decays calculated from $|A_1(t)|^2$ with $t\geq 0$, $t\geq\tau/2$, and $t\geq\tau$ are 22%, 4%, and 1% slower than the real case.

In deducing D from fitting our experimental data with $|A_1(t)|^2$, we recognized the poor signal-to-noise ratio at large t. We therefore fit the data with a single exponential starting from $t=0$, knowing that the deduced value of D could be larger than the real value by about 22%. This is especially true for the lower temperature cases, where less data with $t>\tau/2$ are available because of larger τ. These systematic errors could have reduced the diffusion activation energies and the preexponential factors by 10% and 50%, respectively.

C. Coverage dependence of diffusion coefficient

The diffusion coefficient generally also depends on the surface coverage of adsorbates which we have neglected in our data analysis. If the dependence of D on θ is strong and the grating groove depth is deep, then even with $\Delta\chi^{(2)}_{\rm eff}(\theta)$ linear in θ, the first-order SH diffraction will not have a single exponential decay. This is seen as follows.

Assume $D(\theta)$ can be described by a power series

$$D(\theta)=D(\theta_0)[1+d_1(\theta-\theta_0)+d_2(\theta-\theta_0)^2+\cdots]\ . \quad (21)$$

From Eqs. (8) and (9), we find,

$$\frac{\partial\theta_1}{\partial t}=-\frac{\pi^2}{a^2}D(\theta_0)[\theta_1+\tfrac{1}{2}d_1\theta_1\theta_2+\tfrac{1}{4}d_2\theta_1^3+\cdots]\ ,$$
$$\frac{\partial\theta_2}{\partial t}=-\frac{4\pi^2}{a^2}D(\theta_0)[\theta_2+\tfrac{1}{4}d_1\theta_1^2-\tfrac{11}{8}d_1\theta_1\theta_3,\ldots]\cdots\ . \quad (22)$$

It is obvious that the solution of Eq. (22) will give a $\theta_1(t)$ with a nonexponential or multiexponential decay. Thus even if $\Delta\chi^{(2)}_{\rm eff}(\theta)\propto(\theta-\theta_0)$ so that $A_1(t)=(d\Delta\chi^{(2)}_{\rm eff}/d\theta)_{\theta_0}\theta_1(t)$ from Eq. (13), the first-order SH diffraction may decay nonexponentially. However, if $d_1\theta_1\theta_2$ and the higher-order terms in Eq. (22) are much smaller than θ_1, we still have

$$\frac{\partial\theta_1}{\partial t}\cong-\frac{\pi^2}{a^2}D(\theta_0)\theta_1$$

and hence $\theta_1(t)\propto\exp(-t/2\tau)$, from which $D(\theta_0)$ can be deduced. This can be achieved with a sufficiently small θ_2 either from a shallow monolayer grating with a small initial θ_2^0 or by waiting long enough for θ_2 to decay to a small value.

In our experiment, the CO monolayer grating was square-wave-like with a modulation ranging from zero to full coverage. We estimated $\theta_2^0\sim 0.1$. The fact that the decay of SH diffraction can be roughly fit by single exponentials suggests $d_1\ll 20$ and $d_2\ll 4$. The values of $D(\theta_0)$ deduced from the experiment are accurate to within a factor of 5 judging from the above discussion.

D. Defect of surface effects

Before we discuss the results of our surface diffusion measurements, we need to known whether they are intrinsic to the Ni(110) surface or dominated by defects on the surface. First, consider the effect of point defects. Their density is typically around 10^{-3} to 10^{-4} of a full monolayer.[28] These defect sites are often first covered by adsorbates because of the stronger binding energy. In our experiment with an average coverage of $\theta_0\sim 0.5$, the effect of such point defects is certainly negligible. The same argument can apply to short line defects (ineffective in blocking diffusion paths) with lengths much shorter than the size of the grating.

Special attention has to be paid to line defects which run across the sample and are parallel to the adsorbate grating. They can be steps arising from a miscut of the sample. For diffusion perpendicular to the steps, we have to consider the durations that the adsorbate molecules spend on the terraces and in traversing the steps. Let the average trapping times of an adsorbate molecule on a terrace and at a step site be τ_T and τ_S, respectively. The total time for the molecule to diffuse across a terrace and a step is simply the sum

$$\tau_{\rm tot}=\tau_T+\tau_S\ . \quad (23)$$

If Na is the average width of a terrace, a the lattice constant and also the width of the steps, and N the average number of rows of atoms in a terrace, then from $\langle x^2\rangle=2Dt$, we have $(N+1)^2a^2=2D\tau_{\rm tot}$. With D_T and D_S denoting the diffusion coefficients of adsorbates diffusing on a terrace and across a step, respectively, we also have $N^2a^2=2D_T\tau_T$ and $a^2=2D_S\tau_S$. We then find

$$\frac{1}{D}=\frac{2\tau_{\rm tot}}{(N+1)^2a^2}=\frac{N^2}{(N+1)^2}\frac{1}{D_T}+\frac{1}{(N+1)^2}\frac{1}{D_S}\ . \quad (24)$$

For the steps to dominate in the surface diffusion, we must have $D_S\ll D_T/N^2$.

In our case, the Ni(110) surface had a 0.3° miscut along the [001] direction. This leads to an average terrace width of $N\sim 70$. If we assume that the trial frequencies (preexponential factors in D) for crossing a step and

jumping over an activation energy barrier on a terrace are roughly the same, then $D_S \ll D_T/N^2$ leads to

$$\gamma \equiv N^2 D_S/D_T = 70^2 \exp\{[E_{\text{diff}}(\text{terrace}) - E_{\text{diff}}(\text{step})]/k_B T\} \ll 1 , \quad (25)$$

where E_{diff}(terrace) and E_{diff}(step) are the diffusion activation energies on a terrace and across a step, respectively. If what we measured in our experiment were a step-dominated diffusion process ($\gamma \ll 1$) with $E_{\text{diff}}(\text{step}) = 3.1$ kcal/mol as obtained by fitting $D = D_0 \exp(-E_{\text{diff}}/k_B T)$ to the diffusion data along [001], then Eq. (25) dictates E_{diff}(terrace) should be smaller than [E_{diff}(step) -8.5 kT], which at $T = 150$ K is 0.56 kcal/mol. This small value of E_{diff}(terrace) is only twice as much as the thermal energy (0.3 kcal/mol) and would make the stable adsorption of CO on top- and short-bridge sites of Ni(110) unlikely, contrary to the experimental observation. Therefore, we believe that the measured diffusion is intrinsic for CO on Ni(110) with $\gamma \gg 1$, and the effect of line defects is not significant. If we assume $\gamma = 10$ we estimate from Eq. (24) that $E_{\text{diff}}(\text{step}) \sim 6$ kcal/mol.

E. Anisotropy in diffusion activation energies

Our experimental results described in Sec. III show that there are two independent diffusion barriers, one along $[1\bar{1}0]$ and the other along [001], for CO on Ni(110). The ratio of $E_{\text{diff}}[001]/E_{\text{diff}}[1\bar{1}0]$ is nearly a factor of 3. Such a large anisotropy in the diffusion activation energy can be qualitatively explained by the surface structure of Ni(110). The atomic arrangement of Ni(110) is shown in Fig. 1. The Ni atoms form closely packed rows along [001]. One therefore expects that the surface potential corrugation seen by CO is less along $[1\bar{1}0]$ than along [001] and hence the CO diffusion is faster along $[1\bar{1}0]$.

As we mentioned earlier, it is known that in the coverage range $0 < \theta < 0.85$, CO molecules adsorb on Ni(110) at both top- and short-bridge sites with nearly equal probability.[19] Although there exists some controversy to the occupation ratio of the two sites, θ_t/θ_b, the very weak dependence of this ratio on temperature from 300 to 500 K strongly suggests that the adsorption energy difference between the two sites is small.[19] Our LEED observation of a 3×1 ordered structure of CO adlayer at $\theta = 0.65$ on Ni(110) at ~ 100 K also supports the equal probability assertion as it is explained by equal CO occupation of the top and short-bridge sites.[22] These facts indicate that the surface potential wells for CO at the top and short-bridge sites have about the same depth. That $E_{\text{diff}}[001] \sim 3E_{\text{diff}}[1\bar{1}0]$ is then the result of a strong overlap of neighboring potential wells along $[1\bar{1}0]$, making the energy barrier between adsorption sites along $[1\bar{1}0]$ lower. The above picture is also supported by the observation of streaklike $c(4\times2)$ and $c(8\times2)$ LEED patterns by Behm, Ertl, and Penka,[21] which was interpreted as a consequence of CO occupation at intermediate positions other than the high-symmetry sites (on-top and short-bridge sites) along the $[1\bar{1}0]$ direction.

We can then assume a surface potential seen by CO on Ni(110) to have a form (shown in Fig. 9),[12]

$$V(x,y) = E_{\text{diff}}[1\bar{1}0]\left[1-\cos\frac{4\pi x}{a}\right] + E_{\text{diff}}[001]\left[1-\cos\frac{\sqrt{2}\pi y}{a}\right], \quad (26)$$

with $\hat{x} \| [1\bar{1}0], \hat{y} \| [001]$, and a is the Ni lattice constant of Ni along $[1\bar{1}0]$. Using this potential and the measured values of $E_{\text{diff}}[1\bar{1}0]$ and $E_{\text{diff}}[001]$, we can estimate the fundamental vibrational frequencies for CO trapped at the bottom of such a potential well. They are given by $f_x = (2/a)(E_{\text{diff}}[1\bar{1}0]/M)^{1/2}$ for vibration in $\hat{x}$ and $f_y = (1/\sqrt{2}a)[E_{\text{diff}}[001]/M])^{1/2}$ for vibration in $\hat{y}$, with M taken as the mass of the CO molecule. The estimated values are $f_x \sim 3.3\times10^{12}$ Hz (110 cm^{-1}) and $f_y \sim 1.9\times10^{12}$ Hz (65 cm^{-1}). These vibrational modes are equivalent to the "frustrated translation" modes of CO on Ni(110) which were measured recently with $\theta = 1$ by electron-energy-loss spectroscopy.[20] The latter experiment found a resonant excitation band between 60 and 113 cm^{-1}. This is in good agreement with the values of f_x and f_y estimated here from the measured values of $E_{\text{diff}}[1\bar{1}0]$ and $E_{\text{diff}}[001]$.

We should remark that the surface potential here refers to the potential seen by the adsorbate CO with the surrounding substrate atoms completely relaxed and adjusted to the minimum free-energy configuration. This is not the potential seen by CO moving so rapidly that the substrate atoms have no time to adjust. The latter is perhaps what we need to calculate the vibrational frequency of the frustrated translational modes. However, since the displacement of CO in this vibration is small, the frequency change is expected to be small. In any case, the assumed potential in Eq. (26) is only meant to give a crude estimate. There is no reason why $V(x,y)$ should have the sinusoidal form. The real potential is likely to be more complicated.

The relatively smooth surface potential for CO on

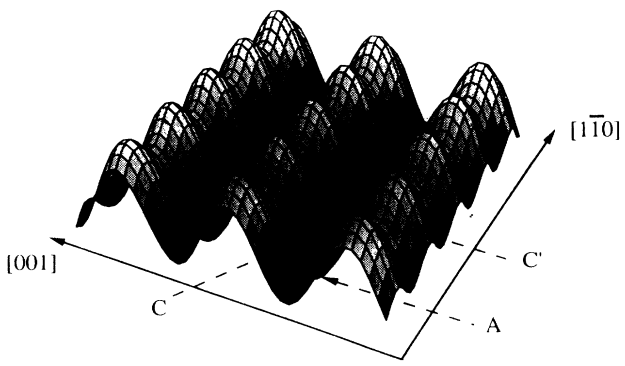

FIG. 9. Surface potential given by Eq. (26). The A position is a potential well and C and C' are the saddle points along $[1\bar{1}0]$ and [001] directions, respectively.

Ni(110) surface characterized by $E_{\text{diff}}[001]=3.1$ kcal/mol and $E_{\text{diff}}[1\bar{1}0]=1.1$ kcal/mol is in strong contrast with CO on the other two low Miller index planes, Ni(111) and Ni(100). For CO on Ni(111), Zhu, Rasing, and Shen and Lin, Lu, and Gomer found $E_{\text{diff}}=6.8$ kcal/mol.[17,29] For CO on Ni(100), Roop *et al.* measured a coverage-dependent E_{diff} of 6.4 kcal/mol for $\theta=0.25$ and 4.6 kcal/mol for $\theta=0.66$.[30] On the other hand, the desorption energies of CO on the three Ni surfaces are not very different: 24 kcal/mol at short-bridge sites and 18 kcal/mol at on-top sites for CO/Ni(111);[31] 21–26 kcal/mol for CO/Ni(100);[32] and 28–32 kcal/mol for CO/Ni(110).[19,25] The ratio of diffusion activation energy to desorption energy is ~0.3 for CO/Ni(111) and CO/Ni(100) cases, while the corresponding ratio for CO/Ni(110) is about 0.1 in the [001] direction and only 0.03 in the $[1\bar{1}0]$ direction.

Theoretical understanding of why the surface potentials of different Ni surfaces are so different is poor. The calculation of Doyen and Ertl[33] for CO on the three Ni surfaces using the molecular-orbital method based on an Anderson-Newns valence-bond formalism is worth mentioning here despite its disagreement with experiment. While it finds a much smoother surface potential (<2 kcal/mol) for CO/Ni(111) than that shown by experiment,[17] it predicts for CO/Ni(110) a surface potential variation of ~2.25 kcal/mol along the [001] direction and ~1.25 kcal/mol along $[1\bar{1}0]$. This seems to agree to some extent with our result on CO/Ni(110). However, the agreement is shadowed by the fact that the calculation suggests the hollow sites as the most stable adsorption sites for CO on Ni(110) which is inconsistent with the result of the recent vibrational spectroscopy study.[20] More refined theoretical calculations, such as the *ab initio* tight-binding calculation by Bullett and Cohen, do exist. They can predict the correct adsorption sites for CO on Ni surfaces but usually not the correct desorption energies and surface potentials.[34] A reliable surface potential calculation for CO on Ni has not yet been carried out.

Although from the surface structure of Ni(110), it is obvious that the diffusion of CO on Ni(110) is anisotropic, yet to the best of our knowledge, the experiment reported here is the first direct observation of an anisotropic heterogeneous chemical surface diffusion with two independent diffusion barriers. In tracer diffusion, there have been a number of experimental studies of anisotropic diffusion on the (110) plane of both bcc and fcc crystals. Adatom diffusion of metal atoms on the (110) plane of fcc crystals such as Ni/Ni(110), Pt/Pt(110), Ir/Pt(110), Ir/Ir/(110), and W/Ir(110) (reviewed by Ehlich and Stolt[3]) are known to have two distinct pathways with the adatoms hopping along the atomic rows of the substrate or exchanging with the substrate atoms (concerted motion) to go across the rows. For chemical diffusion, the case that has been studied is oxygen on W(110). There, only one diffusion pathway along [111] or equivalent directions was identified.[14] From the discussion in this section, we can conclude that the diffusion paths for CO/Ni(110) are as follows: along the $[1\bar{1}0]$ direction, a CO molecule hops successively from a short-bridge (or on-top) site to a neighboring on-top (or short-bridge) site, then to a neighboring short-bridge (or on-top) site, and so on; along the [001] direction, CO hops either from a short-bridge site through a hollow site to another short-bridge site and so on or from an on-top site through a long-bridge site to another on-top site and so on.

F. Anisotropy in preexponential factors: The compensation effect

The experimental results in Sec. III shows that while $E_{\text{diff}}[001]>E_{\text{diff}}[1\bar{1}0]$, the preexponential factor of the diffusion coefficient D_0 is also larger along [001], i.e., $D_0[001]>D_0[1\bar{1}0]$. The consequence is that the two Arrhenius plots for D vs $1/T$ along the $[1\bar{1}0]$ and [001] directions cross each other as seen in Fig. 7. For $T<160$ K, diffusion along [001] is slower than that along $[1\bar{1}0]$, but for $T>160$ K, the reverse is true. A similar behavior has been found with self-diffusion of Ni on the Ni(110) surface.[35] This is a manifestation of a well-known but poorly understood general phenomenon known as "the compensation effect."[36–38] This is, in the Arrhenius form describing the kinetic parameters of related systems, the preexponential factor and the activation energy are related in such a way that if one increases, so will the other. This effect occurs commonly in the kinetics of heterogeneous reactions, including adsorption, desorption, and catalytic reactions,[38] as well as many other thermally activated processes. One example of the latter case is the temperature dependence of the thermally activated electron conductivity of oxide or organic semiconductors, where the compensation effect is also known as the Meyer-Nedel rule.[39] Intuitively, the compensation effect can be understood as follows: The preexponential factor is proportional to the number of ways with which the heat bath can furnish energy to the system to surmount the activation energy barrier. The higher the activation energy, the more ways the system will find by thermal agitation to overcome the energy barrier. Peacock-Lòpez and Suhl have developed a microscopic theory based on this idea to explain the compensation effect.[37]

The similarity of our result to the tracer diffusion of Ni/Ni(110) (Ref. 35) suggests that the adsorbate-adsorbate interaction is not the dominant cause of the compensation. Rather, the interaction of adsorbate-substrate could give rise to this preexponential anisotropy. An argument based on the tracer diffusion can then be used to understand this phenomenon.

The expression for the tracer diffusion coefficient is[40]

$$D=\tfrac{1}{4}\langle l^2\rangle\nu=\tfrac{1}{4}\langle l^2\rangle\nu_0\exp(-E_{\text{diff}}/k_BT)\ , \tag{27}$$

where l is the hopping length, ν the hopping frequency, ν_0 the trial frequency, and E_{diff} the diffusion activation energy. Thus the preexponential factor is defined in terms of hopping length l and trial frequency ν_0 by

$$D_0=\tfrac{1}{4}\langle l^2\rangle\nu_0\ . \tag{28}$$

The anisotropy in D_0 can come from both l and ν_0. Since the diffusion energy barriers are more than 4–8 times larger than the thermal energy kT, it is known both from

molecular-dynamic simulation of atoms (reviewed by Doll and Jacucci[9]) and an analytical estimate[41] that the probability for multiple-lattice hopping is negligible. [A recent molecular-dynamic simulation of molecular carbon monoxide on Ni(111) by Dobb and Doren, however, suggests that such multiple-lattice hopping can be significant.][44] From the previous discussion on diffusion paths, the hopping lengths along the two principal directions, $[1\bar{1}0]$ and [001], are $a/2$ and $\sqrt{2}a$, respectively, with a being the lattice constant along $[1\bar{1}0]$. From Eq. (28) and the measured ratio of $D_0[001]/D_0[1\bar{1}0]$, we then obtain

$$\frac{\nu_0[001]}{\nu_0[1\bar{1}0]} \sim 10^{2\pm1} .$$

In the transition state theory for tracer surface diffusion,[42] the hopping frequency is given by

$$\nu = \nu_0 \exp\left[-\frac{E_{\text{diff}}}{kT}\right] , \tag{29}$$

with

$$\nu_0 = \frac{kT}{h}\frac{Q_C}{Q_A} ,$$

where Q_C is the partition function of the adsorbate (excluding the reaction coordinate) at the saddle point C and Q_A is the total partition function of the adsorbate in the well A (see Fig. 9). We then have

$$\frac{\nu_0[001]}{\nu_0[1\bar{1}0]} = \frac{Q_{C'}[001]}{Q_C[1\bar{1}0]} .$$

In principle, $Q_{C'}/Q_C$ can be calculated if the energy states of all degrees with CO at the saddle points C and C' are known. This is unfortunately not the case for CO on Ni(110). For example, the surface potential for CO/Ni(110) is not available. The one assumed in Eq. (26) is certainly not expected to be valid around the saddle points. A different potential well around a saddle point leads to a different set of vibrational states for CO at that point and hence a very different value of the partition function for that vibrational degree of freedom. For this reason, we find it meaningless to even estimate the ratio $Q_{C'}/Q_C$ unless a reliable surface potential becomes available. This being the case, we are forced to be satisfied with the above-mentioned qualitative explanation for the compensation effect observed in the anisotropy of D_0.

VI. CONCLUSION

We have described here the details of the technique using SH diffraction from a monolayer grating to measure surface diffusion. The technique is applicable to all surfaces and is ideal for studying diffusion on crystalline surfaces with strong anisotropy. The anisotropic surface diffusion of CO/Ni(110) is used as a demonstration. The results indicate unequivocally the existence of two independent diffusion barriers along [001] and $[1\bar{1}0]$. The activation energies and the preexponential factors for the two orthogonal directions are deduced from the measured diffusion coefficients. A strong anisotropy in surface diffusion of CO/Ni(110) is found. The significantly smaller activation energy for diffusion along $[1\bar{1}0]$ is directly associated with the close-packed rows of Ni atoms along $[1\bar{1}0]$. The preexponential factors exhibit the common "compensation effect" for thermally activated process. In comparison with CO/Ni(111) and CO/Ni(110), the surface diffusion results suggest that the Ni(110) surface seen by CO is much smoother than Ni(111) and Ni(100), although the desorption energies of CO on these three Ni surfaces are comparable. The various effects that may influence the data analysis are discussed.

As seen from the work described here, the monolayer grating technique has clearly the advantage of involving a simple and straightforward data analysis. This eliminates the need of developing a theory just for the data analysis as with some other techniques. However, the present method using SH diffraction to probe the monolayer grating often suffers from a poor signal-to-noise ratio. This makes the study of, for example, coverage dependence of surface diffusion difficult. It is possible to greatly enhance the signal-to-noise ratio by using linear optical diffraction instead to probe the monolayer grating.[43] The coverage dependence of surface diffusion which we have neglected in the present work can then be measured. Research in this direction is presently being carried out in our laboratory.

ACKNOWLEDGMENTS

One of the authors (W.D.) gratefully acknowledges support by the Alexander von Humboldt Foundation, Federal Republic of Germany. This work was supported by the Director, Office of Energy Research, Office of Basic Energy Sciences, Materials Sciences Division of the U.S. Department of Energy under Contract No. DE-ACO3-76SF00098.

*Permanent address: Department of Physics, University of California, Davis, CA 95616.

†Permanent address: Institute für Grenzflächenforschung and Vakuumphysik, Kernforschungsanlage Jülich, D-5170 Jülich, Germany.

[1]An excellent review of the field has been provided recently by R. Gomer, Rep. Prog. Phys. **53**, 917 (1990).

[2]A. G. Naumovets and Yu. S. Vedula, Surf. Sci. Rep. **4**, 365 (1985).

[3]G. Ehlich and Kaj Stolt, Ann. Rev. Phys. Chem. **31**, 603 (1980).

[4]Y. W. Mo, J. Kleiner, M. B. Webb, and M. G. Lagally, Phys. Rev. Lett. **66**, 1998 (1991).

[5]J. D. Doll and H. K. McDowell, J. Chem. Phys. **77**, 479 (1982).

[6]G. De Lorenzi and G. Jacucci, Surf. Sci. **116**, 391 (1982).

[7]M. R. Mruzik and G. M. Pound, J. Phys. F **11**, 1403 (1981).

[8]Arthur F. Voter and Jimmie D. Doll, Chem. Phys. **82**, 80 (1985).

[9]C. P. Flynn and G. Jacucci, Phys. Rev. B **25**, 6225 (1982).

[10]J. D. Doll and A. F. Voter, Ann. Rev. Phys. Chem. **38**, 413 (1987).

[11]Goran Wahnstrom, Surf. Sci. **159**, 311 (1985).
[12]S. C. Ying, Phys. Rev. B **41**, 7068 (1990); Tapio Ala-Nissila and S. C. Ying, Phys. Rev. Lett. **65**, 879 (1990); I. C. da Cunha Lima, A. Troper, and S. C. Ying, Phys. Rev. B **41**, 11 798 (1990).
[13]D. Ghaleb and B. Perraillon, Surf. Sci. **162**, 103 (1985).
[14]M. Tringide and R. Gomer, Surf. Sci. **155**, 254 (1985); **166**, 419 (1986).
[15]For example, A. A. Deckert, J. L. Brand, M. V. Arena, and S. M. George, Surf. Sci. **208**, 441 (1989); C. H. Mak, J. L. Brand, B. G. Koehler, and S. M. George, *ibid.* **191**, 108 (1987), and references therein.
[16]J. N. Russell, Jr. and R. B. Hall, Surf. Sci. **203**, L642 (1988).
[17]X. D. Zhu, Th. Rasing, and Y. R. Shen, Phys. Rev. Lett. **61**, 2883 (1988).
[18]Xu-dong Xiao, X. D. Zhu, W. Daum, and Y. R. Shen, Phys. Rev. Lett. **66**, 2352 (1991).
[19]J. Bauhofer, M. Hock, and J. Kuppers, Surf. Sci. **191**, 395 (1987).
[20]B. Voigtlander, S. Lehwald, and H. Ibach, Surf. Sci. **225**, 151 (1990).
[21]R. J. Behm, G. Ertl, and V. Penka, Surf. Sci. **160**, 387 (1985).
[22]X. D. Zhu, Winfried Daum, Xu-dong Xiao, R. Chin, and Y. R. Shen, Phys. Rev. B **43**, 11 571 (1991).
[23]X. D. Zhu, Ph.D. thesis, Berkeley, 1989.
[24]*American Institute of Physics Handbook,* 3rd ed., edited by D. Gray (McGraw-Hill, New York, 1972), pp. 4-106 and 4-154.
[25]C. S. Feigerle, S. R. Desai, and S. H. Overbury, J. Chem. Phys. **93**, 787 (1990).
[26]X. D. Zhu, and Y. R. Shen, Opt. Lett. **14**, 503 (1989).
[27]J. C. Hamilton, R. J. M. Anderson, and L. R. Williams, J. Vac. Sci. Technol. B **7**, 1203 (1989).
[28]J. E. Reutt-Robey, D. J. Doren, Y. J. Chabal, and S. B. Christman, Phys. Rev. Lett. **61**, 2778 (1988).
[29]T.-S. Lin, H.-J. Lu, and R. Gomer, Surf. Sci. **234**, 251 (1990).
[30]B. Roop, A. Costello, D. R. Mullins, and J. M. White, J. Chem. Phys. **86**, 3003 (1987).
[31]J. B. Miller, H. R. Siddiqui, S. M. Gates, J. N. Russell, Jr., J. T. Yates, Jr., J. C. Tully, and M. J. Cardillo, J. Chem. Phys. **87**, 6725 (1987).
[32]J. T. Yates and D. W. Goodman, J. Chem. Phys. **73**, 5371 (1980).
[33]G. Doyen and G. Ertl, Surf. Sci. **43**, 197 (1974).
[34]D. W. Bullett and M. L. Cohen, Solid State Commun. **21**, 157 (1977); K. W. Frese, Jr., Surf. Sci. **202**, 277 (1988).
[35]Raymond T. Tung, and William R. Graham, Surf. Sci. **97**, 73 (1980).
[36]P. J. Estrup, E. F. Greene, M. J. Cardillo, and J. C. Tully, J. Chem. Phys. **90**, 4099 (1986).
[37]E. Peacock-López and H. Suhl, Phys. Rev. B **26**, 3774 (1982).
[38]A. K. Galwey, Adv. Catal. **26**, 247 (1977).
[39]W. Meyer and H. Nedel, Z. Tech. Phys. **18**, 588 (1937); H. C. Eror and J. B. Wagner, Phys. Status Solidi **35**, 641 (1969); D. D. Eley, J. Polym. Sci. C **17**, 73 (1967).
[40]*Surface Mobilities on Solid Materials,* edited by Vu Thien Binh (Plenum, New York, 1983).
[41]V. P. Zhdanov, Surf. Sci. **214**, 289 (1989); **161**, L614 (1985).
[42]Jack G. Landerdale and Donald G. Truhlar, Surf. Sci. **164**, 558 (1985).
[43]Xu-dong Xiao, Yuanlin Xie, and Y. R. Shen, Surf. Sci. **271**, 295 (1992).
[44]D. J. Doren, Bull. Am. Phys. Soc. **37**, 527 (1992); K. D. Dobbs and D. J. Doren (unpublished).

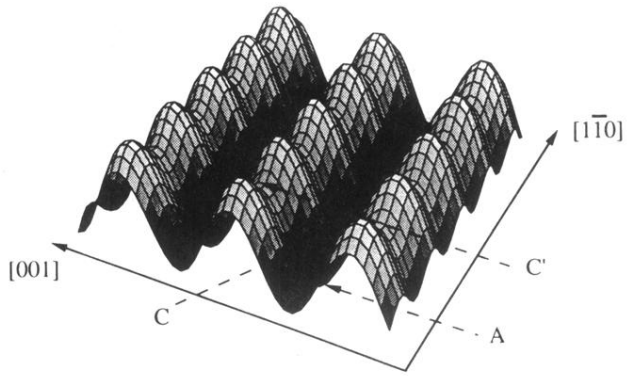

FIG. 9. Surface potential given by Eq. (26). The A position is a potential well and C and C' are the saddle points along [1$\bar{1}$0] and [001] directions, respectively.